High Throughput Screening of Magnetic Antiperovskites

Harish K. Singh,*[,†] Zeying Zhang,[§,†] Ingo Opahle,*[,†] Dominik Ohmer,[†] Yugui Yao,[§] and Hongbin Zhang*[,†]

[†] Institute of Materials Science, TU Darmstadt, Otto-Berndt-Str. 3, 64287 Darmstadt, Germany

[§] Beijing Key Laboratory of Nanophotonics and Ultrafine Optoelectronic Systems, School of Physics, Beijing Institute of Technology, Beijing 100081, China

Supporting Information

Table S1. The experimentally reported antiperovskites in the $Pm\bar{3}m$ space group. Second and third column represents the comparison between the calculated and experimentally reported lattice parameters (Å). The calculated ferromagnetic and non-magnetic (NM) ground state are listed in forth column. The formation energy (eV/atom) of antiperovskites are listed in fifth column. The distance to the convex hull (eV/atom) of APVs are listed in last column.

Compounds	Calculated Lattice Constant (Å)	Experimental Lattice Constant (Å)	Magnetic moment (BM/f.u.)	Formation energy (eV/atom)	Convex Hull (eV/atom)
Co_3CdN	3.84	3.841[85]	3.24	-0.050	0.000
Co_3CuN	3.73	3.75[86]	4.07	-0.042	0.005
Co_3GeN	3.77	3.629[8]	3.42	-0.079	0.043
Co_3InN	3.84	3.854[7]	2.72	-0.123	0.022
Co_3MgC	3.77	3.81[84]	1.08	-0.072	0.000
Co_3ZnC	3.73	3.72[62]	1.07	-0.019	0.000
Cr_3GaN	3.83	3.879[87]	NM	-0.329	0.020
Cr_3IrN	3.81	3.843[59]	0.42	-0.365	0.007
Cr_3PdN	3.83	3.889[59]	NM	-0.253	0.081
Cr_3PtN	3.84	3.879[59]	1.46	-0.400	0.000
Cr_3RhN	3.81	3.854[59]	NM	-0.310	0.036
Cr_3SnN	3.94	3.974[59]	0.25	-0.189	0.123
Fe_3AlC	3.75	3.79[88]	3.10	-0.165	0.000
Fe_3AuN	3.89	3.841[89]	7.50	-0.161	0.000
Fe_3GaN	3.79	3.797[90] (3.800)[76]	5.21	-0.255	0.016
Fe_3InN	3.89	3.867[91]	5.50	-0.129	0.012
Fe_3NiN	3.78	3.79[92]	8.01	-0.139	0.025
Fe_3PdN	3.86	3.866[93]	8.25	-0.208	0.000
Fe_3PtN	3.86	3.857[92]	8.19	-0.263	0.000
Fe_3RhN	3.84	3.833[94]	8.77	-0.150	0.000
Fe_3SnC	3.83	3.85[54]	NM	-0.238	0.049
Fe_3SnN	3.89	3.837[95]	5.09	-0.104	0.037
Fe_3ZnC	3.77	3.80[54]	4.10	0.010	0.016
Fe_3ZnN	3.77	3.800[91]	4.76	-0.204	0.000
Fe_4N	3.79	3.790[96]	9.92	-0.121	0.020
Mn_3AgN	4.00	4.020[97]	9.90	-0.158	0.096
Mn_3AlN	3.77	3.854[55]	2.95	-0.454	0.195
Mn_3AuN	4.00	4.024[98]	10.05	-0.312	0.000

Mn_3CuN	3.83	3.904[57, 99]	7.59	-0.186	0.068
Mn_3GaN	3.77	3.898[63]	3.07	-0.376	0.000
Mn_3InC	3.95	3.993[53]	6.03	0.020	0.093
Mn_3InN	4.01	4.029[60]	7.84	-0.184	0.070
Mn_3IrN	3.89	3.913[59]	8.73	-0.217	0.097
Mn_3NiN	3.84	3.886[100]	8.83	-0.224	0.059
Mn_3PdN	3.93	3.979[59]	9.51	-0.307	0.024
Mn_3PtN	3.94	3.972[59]	9.65	-0.387	0.003
Mn_3RhN	3.89	3.938[59]	8.78	-0.228	0.092
Mn_3SnC	3.89	3.989[61]	3.28	-0.014	0.059
Mn_3SnN	3.87	4.060[59]	3.00	-0.221	0.033
Mn_3ZnC	3.87	3.930[61]	7.03	-0.030	0.044
Mn_4N	3.75	3.865[101]	1.21	-0.249	0.005
Ni_3CdC	3.87	3.844[102]	NM	-0.020	0.023
Ni_3CdN	3.86	3.848[85]	NM	-0.187	0.000
Ni_3CuN	3.74	3.742[103]	3.74	-0.094	0.000
Ni_3GaC	3.78	3.6[65]	NM	-0.110	0.000
Ni_3GeC	3.81	3.58[65]	NM	-0.111	0.318
Ni_3InN	3.87	3.844[7]	NM	-0.206	0.000
Ni_3MgC	3.82	3.805[1]	NM	-0.143	0.000
Ni_3ZnN	3.77	3.756[104]	NM	-0.266	0.000
Ni_4N	3.73	3.72[105]	1.57	0.008	0.068

Table S2. The experimentally reported antiperovskites in non-cubic space group. The given data is calculated in the $Pm\bar{3}m$ space group for each compounds in the table. The formation energy (eV/atom) of antiperovskites are calculated in the $Pm\bar{3}m$ (non-cubic space group). The distance to the convex hull (eV/atom) for APVs (M_3XZ) are listed in fourth column. Last column indicates the respective antiperovskite space group.

Compounds	Magnetic moment (BM/f.u.)	Formation energy (eV/atom) $Pm\bar{3}m$ (non-cubic space group)	Convex Hull (eV/atom)	Comment
Cr_3AsC	1.81	0.147 (-0.109)	0.288	Cmcm[68]
Cr_3AsN	2.58	-0.232 (-0.383)	0.157	I4/mcm[59, 66]
Cr_3GeC	5.58	0.069 (-0.058)	0.173	Cmcm[67]
Cr_3GeN	NM	-0.290 (-0.331)	0.056	$P42_1m$[59, 67]
Cr_3PC	NM	0.108 (-0.286)	0.390	Cmcm[68, 74]
Cr_3PN	2.11	-0.283 (-0.558)	0.245	Cmcm[68, 74]

Fe_3GeN	6.13	-0.144 (-0.430)	0.058	I4/mcm[66]
Mn_3AsN	4.51	-0.194	0.167	T4[59]
Mn_3GeC	2.99	-0.054 (-0.132)	0.042	I4/mcm[66]
Mn_3GeN	2.51	-0.292 (-0.314)	0.009	I4/mcm[59, 66]
Mn_3SbN	4.48	-0.132	0.133	P4/mmm[106]
Ni_3FeN	4.16	0.032	0.166	Thin films on $SrTiO_3$[107]

Table S3. Experimentally reported antiperovskites in non-stoichiometric state. The given data is calculated by considering stoichiometric state only. Second and third column represents the comparison between the calculated and experimental reported lattice parameters (Å). The calculated ferromagnetic and non-magnetic (NM) ground state are listed in forth column. The distance to the convex hull (eV/atom) for APVs are listed in sixth column. Last column represents the dynamical stability.

Compounds	Calculated Lattice Constant (Å)	Experimental Lattice Constant (Å)	Magnetic moment (BM/f.u.)	Formation energy (eV/atom)	Convex Hull (eV/atom)	Dynamical Stability
$Co_3AlC_{0.59}$	3.72	3.69[84]	NM	-0.359	0.000	Unstable
$Co3GaC_{0.5}$	3.73	3.65[65]	NM	-0.236	0.000	Unstable
$Co_3GeC_{0.25}$	3.75	3.6[62]	1.76	0.055	0.139	Unstable
$Co_3InC_{0.75}$	3.83	3.86[62]	NM	-0.128	0.099	Stable
Co_3ScC_{1-X}	3.81	3.827[108]	NM	-0.427	0.000	Stable
$Co_3SnC_{0.7}$	3.84	3.77[54]	1.68	0.013	0.058	Stable
$Fe_{3.64}Ag_{0.36}N$	3.88	3.800[89]	7.38	-0.050	0.091	Stable
$Mn_3CoN_{0.74}$	3.82	3.879[73]	9.26	-0.156	0.099	Unstable
$Mn_3Al_{0.9}C$	3.80	3.871[109]	3.99	-0.187	0.000	Stable
$Mn_3Ga_{0.97}C$	3.81	3.897[109]	4.16	-0.110	0.000	Stable
$Mn_3Zn_{0.80}N$	3.79	3.912[110]	4.24	-0.284	0.000	Stable
$Ni_3AlC_{0.29}$	3.77	3.61[83]	NM	-0.218	0.164	Unstable
$Ni_3InC_{0.50}$	3.87	3.78[62]	NM	-0.073	0.038	Stable
$Ni_3ZnC_{0.7}$	3.77	3.65[54]	NM	-0.093	0.042	Stable

Table S4. The novel antiperovskites with convex hull distance >50-100< meV/atom. The given compounds satisfy the mechanical and dynamical stability criteria. The second column correspond to the ground state (GS) lattice parameter and third column listed the lattice constant in NM state. Fourth column represents the ground state of APVs. The distance to the convex hull (eV/atom) for APVs are listed in fifth column. The given data is calculated in the $Pm\bar{3}m$ space group for each compounds in the table.

Compounds	GS Lattice Constant (Å)	NM Lattice Constant (Å)	Magnetic moment (BM/f.u.)	Formation energy (eV/atom)	Convex Hull (eV/atom)
Co_3FeN	3.74	3.68	7.43	-0.082	0.052
Co_3MgN	3.78	3.76	2.80	-0.209	0.086
Co_3MnN	3.75	3.69	7.81	-0.133	0.064
Co_3YC	3.91	3.91	NM	-0.290	0.059
Cr_3MoN	3.84	3.84	4.83	-0.204	0.101
Cr_3PtC	3.85	3.85	NM	-0.053	0.088
Cr_3ZnN	3.82	3.82	NM	-0.227	0.086
Fe_3CdN	3.90	3.82	6.43	-0.074	0.066
Fe_3CoN	3.77	3.67	8.91	-0.108	0.058
Fe_3HfC	3.81	3.82	NM	-0.554	0.099
Fe_3MnN	3.68	3.72	10.65	-0.088	0.100
Fe_3TaC	3.78	3.78	0.88	-0.127	0.092
Fe_3TiC	3.74	3.74	NM	-0.522	0.097
Mn_3AuC	3.97	3.83	8.63	-0.008	0.088
Mn_3CdN	4.02	3.85	9.36	-0.164	0.090
Mn_3MoN	3.77	3.77	NM	-0.203	0.051
Mn_3NbC	3.83	3.84	1.39	-0.106	0.093
Mn_3PtC	3.92		8.51	-0.077	0.098
Mn_3ScC	3.90	3.87	3.99	-0.125	0.072
Mn_3TaC	3.82	3.82	1.34	-0.148	0.090
Mn_3WC	3.78	3.78	NM	0.000	0.092
Ni_3MnN	3.79	3.73	5.25	-0.100	0.097

Table S5. The novel antiperovskites fails to obey the dynamical stability criteria but satisfy the thermodynamical and mechanical stability. The given compounds satisfy the thermodynamical and mechanical stability criteria only. The second column corresponds to the ground state (GS) lattice parameter. The distance to the convex hull (eV/atom) for APVs (M_3XZ) are listed in fifth column. The given data is calculated in the $Pm\bar{3}m$ space group for each compounds in the table.

Compounds	GS Lattice Constant (Å)	Magnetic moment (BM/f.u.)	Formation energy (eV/atom)	Convex Hull (eV/atom)
Co_3NiN	3.72	5.1	-0.038	0.014
Co_4N	3.72	6.3	-0.004	0.043
Cr_3IrC	3.83	0.00	-0.030	0.104
Cr_3MnN	3.81	-0.89	-0.242	0.071

Cr_3OsN	3.81	0.01	-0.243	0.069
Cr_3ReN	3.82	0.03	-0.227	0.086
Cr_3RuN	3.80	0.01	-0.244	0.068
Cr_3TcN	3.81	0.01	-0.237	0.075
Fe_3GaC	3.76	3.16	-0.063	0.044
Fe_3ScC	3.85	3.0	-0.162	0.022
Mn_3CrN	3.76	0.89	-0.216	0.068
Mn_3TcN	3.75	0.01	-0.160	0.094
Mn_3WN	3.77	0.02	-0.191	0.063
Ni_3AgN	3.83	0.8	-0.067	0.000
Ni_3AuN	3.84	0.7	-0.106	0.000
Ni_3CaC	3..96	0.22	-0.027	0.095
Ni_3GaN	3.78	0.02	-0.218	0.063
Ni_3HgN	3.88	0.0	-0.065	0.000
Ni_3LiN	3.75	0.9	-0.235	0.007
Ni_3MgN	3.82	0.0	-0.291	0.044
Ni_3MnN	3.79	5.25	-0.100	0.097
Ni_3PdN	3.80	1.3	-0.074	0.000
Ni_3PtN	3.80	0.4	-0.067	0.011
Ni_3ScC	3.88	0.0	-0.254	0.086
Ni_3SnN	3.90	0.00	-0.085	0.077

Table S6. Elastic constant for the Ni_3XC (X = Y, Zr, Nb, Mo, Tc, Ru, Rh, Pd, Ag) antiperovskites. Parenthesis elastic constant correspond to the Banikkov[35] et al. Work and Shen work[70] (Cd).

Compound	C_{11} (GPa)	C_{12} (GPa)	C_{44} (GPa)
Ni_3AgC	309.1 (251.43)	128.8 (108.12)	28.9 (19.04)
Ni3CdC	305.7 (311.5)	124.9 (126.7)	55.5 (57.2)
Ni_3MgC	314.94 (309.47)	106.27 (101.84)	40.72 (42.64)
Ni_3MoC	342.7 (325.78)	171.0 (163.28)	-5.1 (-12.29)
Ni_3NbC	321.6 (278.91)	166.4 (144.59)	2.08 (-3.67)
Ni_3PdC	315.3 (290.09)	151.9 (128.42)	36.56 (45.59)
Ni_3RhC	358.9 (348.87)	144.4 (144.70)	39.5 (52.05)
Ni_3RuC	372.4 (361.84)	159.3 (144.58)	46.2 (59.31)
Ni_3TcC	356.8 (354.00)	162.5 (148.41)	32.1 (37.71)
Ni_3YC	275.9 (285.02)	114.7 (95.36)	11.6 (20.32)

Ni_3ZnC	343.31 (319.53)	116.26 (105.72)	40.23 (39.42)
Ni_3ZrC	329.1 (313.99)	132.1 (114.37)	15.3 (18.09)

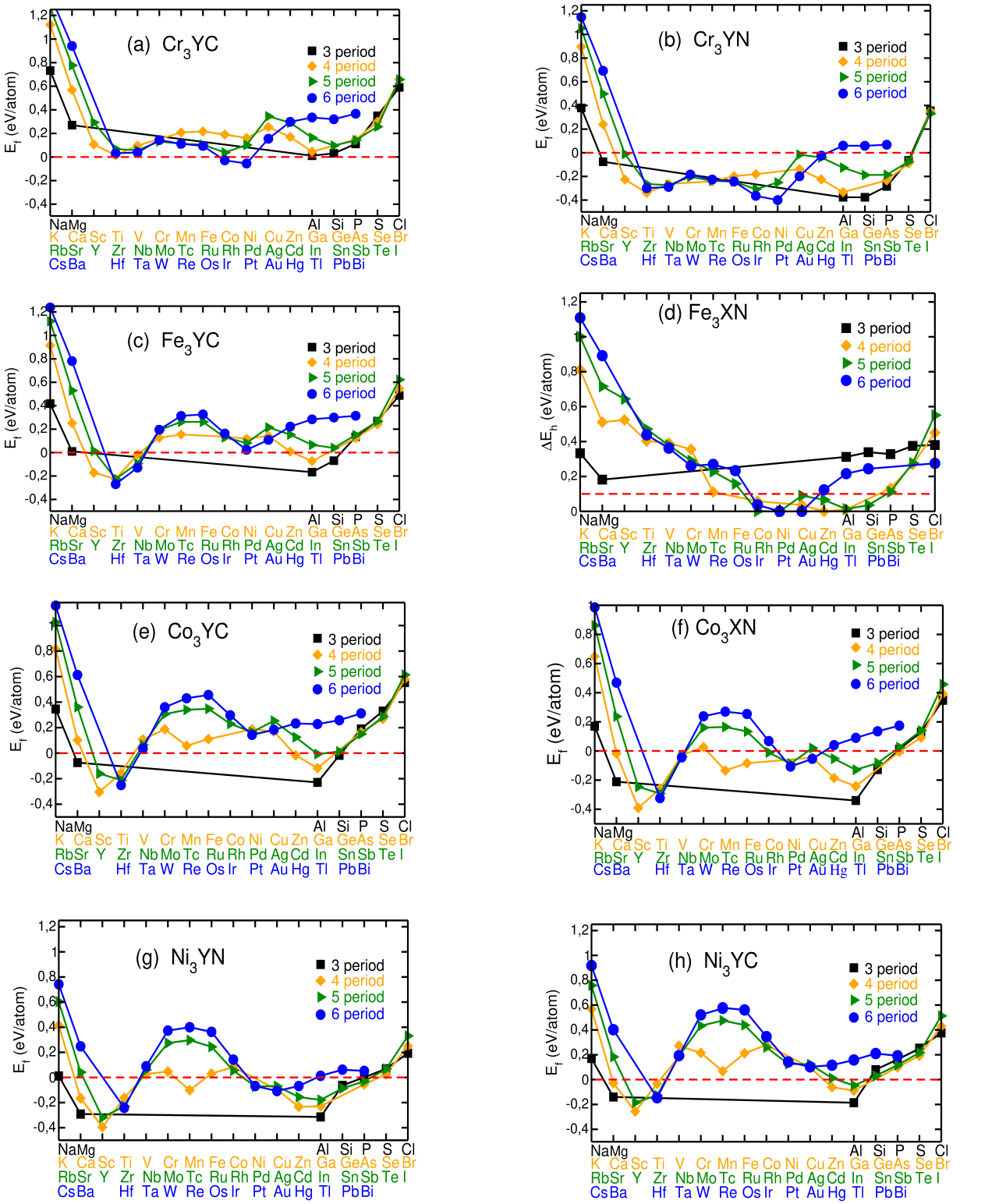

Figure S1: The formation energies of the antiperovskites M_3XZ, where X belongs to the elements present on the x-axis of each plot.

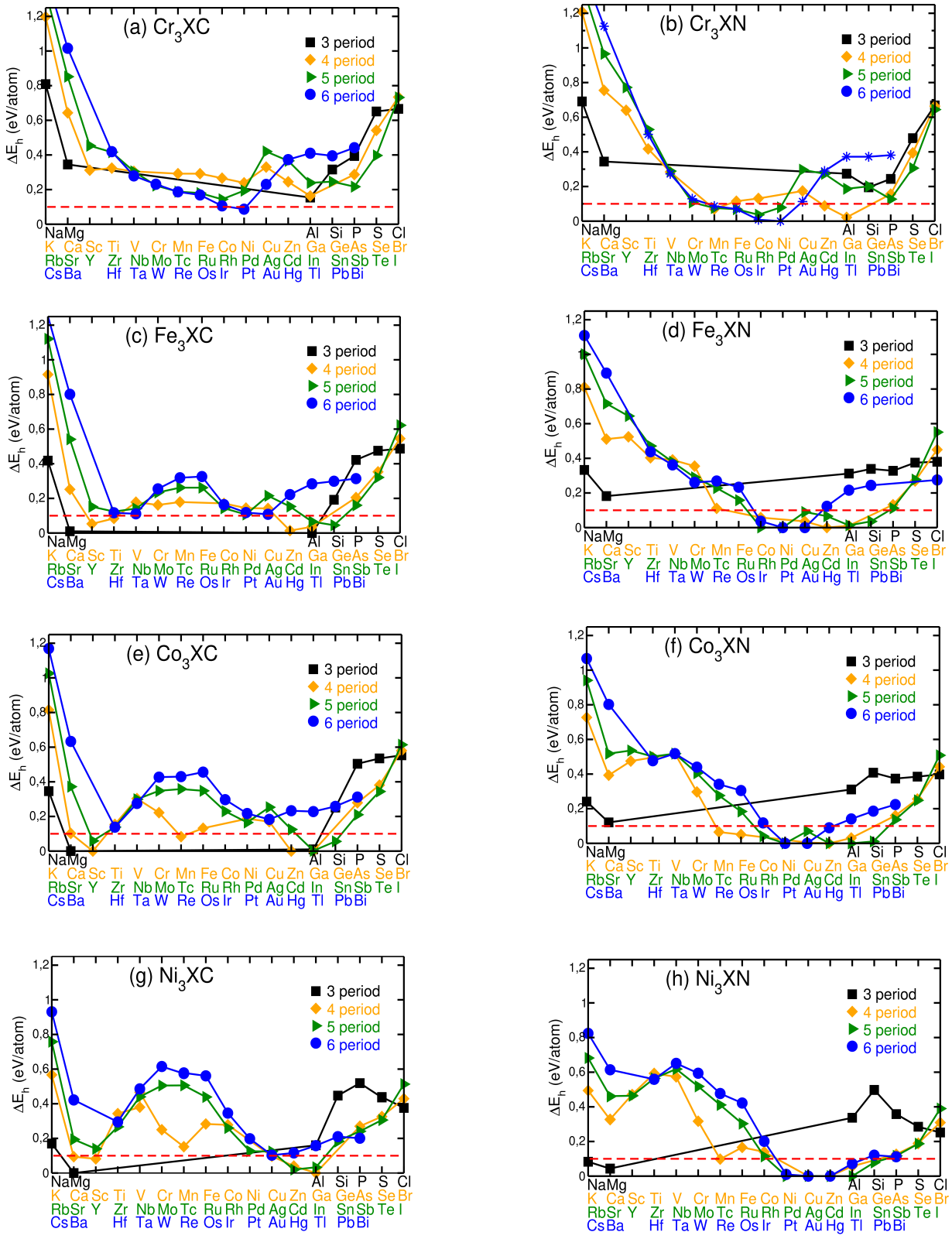

Figure S2: The convex hull distance of the antiperovskites M_3XZ, where X belongs to the elements present on the x-axis of each plot.

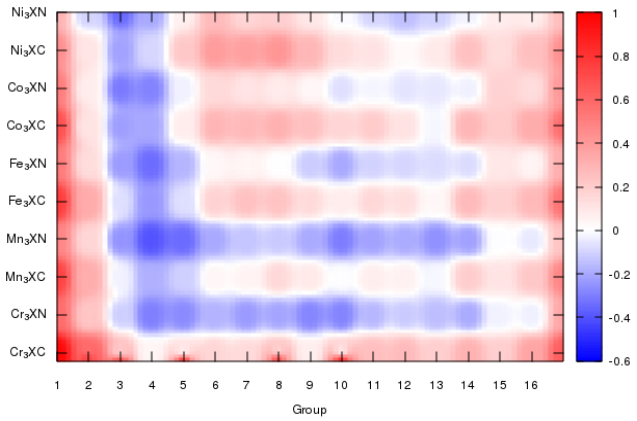

Figure S3. The correlation plot for antiperovskites, where y-axis is formation energy (eV/atom) for respective antiperovskites present on the y-axis. The x-axis indicated the elements X of the respective group of the periodic table. The x-axis also represents the number of valence electrons, the group 1-12 contains same number of valence electron as the group number, while 13, 14, 15, 16 and 17 have 3, 4, 5, 6, and 7 valence electrons respectively.

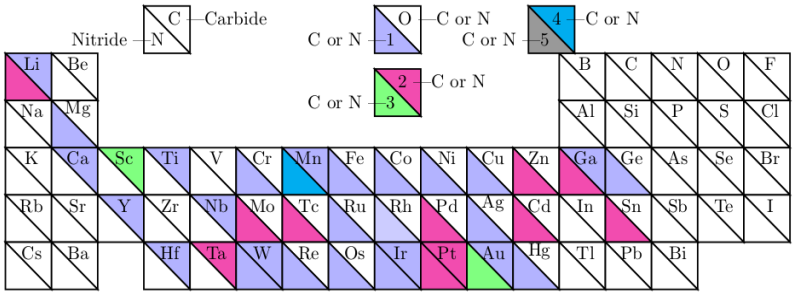

Figure S4. The given novel antiperovskites fulfil the thermodynamical, mechanical stability criteria. Distribution of novel antiperovskites M_3XZ in periodic table. The upper and lower triangular corner represents antiperovskites carbides and nitrides respectively. Each element in the periodic table represents X for the chemical formula M_3XZ where M = Cr, Mn, Fe, Co and Ni. The color indicates the number of stable phases for each X element.

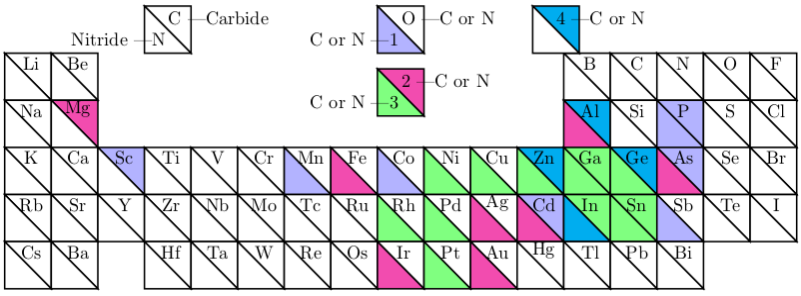

Figure S5. Distribution of experimental antiperovskites M_3XZ. The upper and lower triangular corner represents antiperovskites carbides and nitrides respectively. Each element in the periodic table represents X for the chemical formula M_3XZ where M = Cr, Mn, Fe, Co and Ni. The color indicates the number of stable phases for each X element.

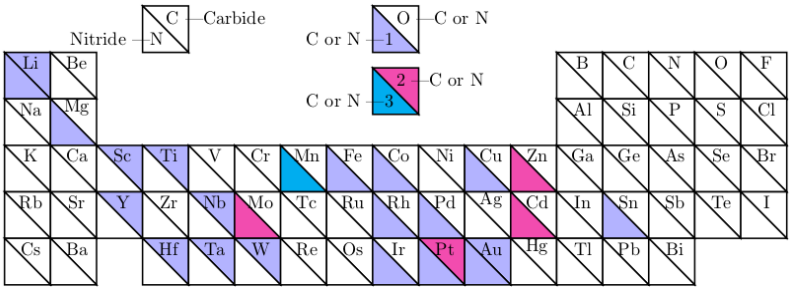

Figure S6: Distribution of unreported APVs M_3XZ with ΔE_h < 100 meV/atom. The upper and lower triangular corner represents APVs carbides and nitrides respectively. Each element in the periodic table represents X for the chemical formula M_3XZ where M = Cr, Mn, Fe, Co and Ni. The color indicates the number of stable phases for each X element. The given APVs fulfil the thermodynamical, mechanical and dynamical stability criteria.

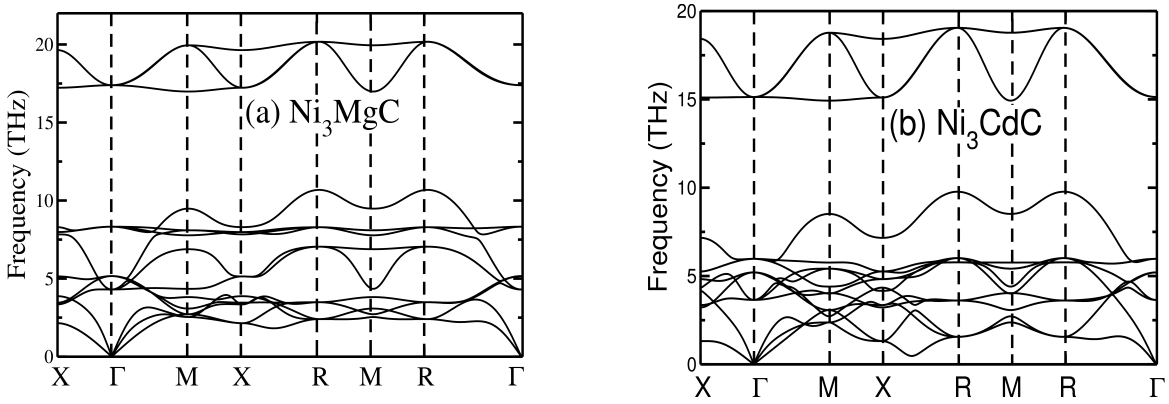

Figure S7: The calculated phonon dispersion for (a) Ni_3MgC and (b) Ni_3CdC antiperovskites.

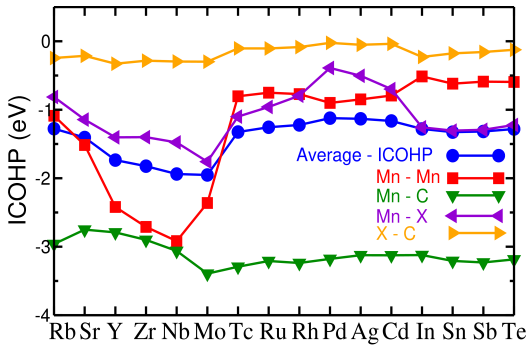

Figure S8: The integrated chemical orbital Hamilton population (ICOHP) of the APV M_3XC, where X belongs to the set of elements shown as labels of the x-axis for each plot.

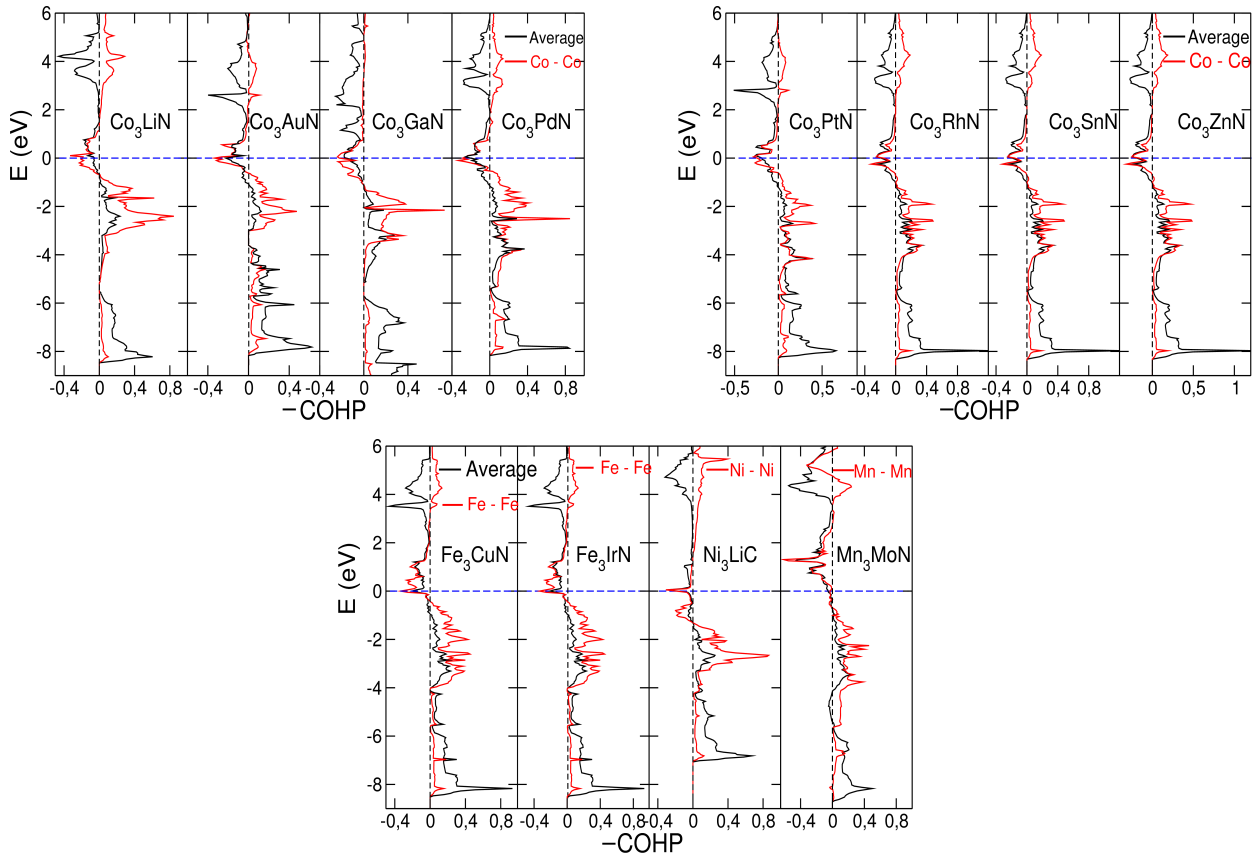

Figure S9: The non-spin polarized chemical orbital Hamilton population (COHP) curves for the M_3XZ APVs. The COHP curves include the average bond populations of M_3XZ and M-M bond where M = Cr, Mn, Fe, Co and Ni. The E_f lies at 0 eV which is represented by dotted line (blue). The each COHP plot belongs to the particular APV M_3XZ as mentioned in the plot. The left and right part of the vertical black dotted line represents the antibonding and bonding states respectively.

References:

(83) Han, K. H. C. W.-K. Systematic Arrangement of the Binary Rare-Earth-Aluminium Systems. *Scr. Metall.* **1983**, *17*, 281–284.

(84) Huetter, L. J.; Stadelmaier, H. H. Ternary Carbides of Transition Metals with Aluminum and Magnesium. *Acta Metall.* **1958**, *6*, 367–370.

(85) He, B.; Dong, C.; Yang, L.; Ge, L.; Chen, H. Preparation and Physical Properties of Antiperovskite-Type Compounds $CdNCo_{3-z}Ni_z(0\leq z\leq 3)$. *J. Solid State Chem.* **2011**, *184*, 1939–1945.

(86) Hui, Z.; Tang, X.; Shao, D.; Wei, R.; Yang, J.; Tong, P.; Song, W.; Zhu, X.; Sun, Y. Self-Assembled c-Axis Oriented Antiperovskite Soft-Magnetic $CuNCo_3$ Thin Films by Chemical Solution Deposition. *J. Mater. Chem. C* **2015**, *3*, 4438–4444.

(87) Lin, S.; Tong, P.; Wang, B.; Huang, Y.; Shao, D.; Lu, W.; Sun, Y. P. Synthesis and Characterization of Antiperovskite Nitrides $GaNCr_{3-x}Mn_x$. *J. Solid State Chem.* **2014**, *209*, 127–134.

(88) Putyatin, A. A.; Davydov, V. E.; Nesterenko, S. N. High Temperature Interactions in the Fe-Al-C System at 6 GPa Pressure. *J. Alloys Compd.* **1992**, *179*, 165–175.

(89) de Figueiredo, R. S.; Kuhnen, C. A.; dos Santos, A. V. Crystallographic, Magnetic and Electronic Structure of Iron-Silver and Iron-Gold Perovskite Nitrides. *J. Magn. Magn. Mater.* **1997**, *173*, 141–154.

(90) Houben, A.; Burghaus, J.; Dronskowski, R. The Ternary Nitrides $GaFe_3N$ and $AlFe_3N$: Improved Synthesis and Magnetic Properties. *Chem. Mater.* **2009**, *21*, 4332–4338.
(91) Kuhnen, C. A.; Figueiredo, R. S. De; Santos, A. V. Mössbauer Spectroscopy, Crystallographic, Magnetic and Electronic Structure of $ZnFe_3N$ and $InFe_3N$. *J. Magn. Magn. Mater.* **2000**, *219*, 58–68.
(92) Wiener, G. W.; Berger, J. A. Structure Snd Magnetic Properties of Some Transition Metal Nitrides. *J. Met.* **1955**, *7*, 360–368.
(93) Stadelmaier, H. H.; Fraker, A. C. Nitrides of Iron with Nickel, Palladium and Platinum. *Trans. Metall. Soc. Aime* **1960**, *218*, 571–572.
(94) Houben, A.; Sepelak, V.; Becker, K. D.; Dronskowski, R. Itinerant Ferromagnet $RhFe_3N$: Advanced Synthesis and ^{57}Fe Mossbauer Analysis. *Chem. Mater.* **2009**, *21*, 784–788.
(95) Zhao, Z.; Xue, D.; Chen, Z.; Li, F. Preparation and Characterization of γ'-Fe_3SnN. *Phys. Status Solidi* **1999**, *249*, 249–254.
(96) Jacobs, H.; Rechenbach, D.; Zachwieja, U. Structure Determination of Γ′-Fe_4N and □-Fe_3N. *J. Alloys Compd.* **1995**, *227*, 10–17.
(97) Deng, S.; Sun, Y.; Yan, J.; Shi, Z.; Shi, K.; Wang, L.; Hu, P.; Malik, M. I.; Wang, C. The Evolution of Magnetic Transitions, Negative Thermal Expansion and Unusual Electronic Transport Properties in $Mn_3Ag_xMn_yN$. *Solid State Commun.* **2015**, *222*, 37–41.
(98) Roland, M. M.; Gilles, L.; Rouault, A.; Bouchaud, J-P.; Fruchart, M. E.; Lorthioir, M. M. G.; Fruchart, R. Six Nouveaux Nitrures Lernaires Du Manganese. Etude Des Transitions Du Premier Ordre Dans Les Nitrures et Carbures Complexes de Structure Perovskite. *Comptes rendus Hebd. des séances de Académie des Sci. Série B* **1972**, *264*, 308–311.
(99) Chi, E. O.; Kim, W. S.; Hur, N. H. Nearly Zero Temperature Coefficient of Resistivity in Antiperovskite Compound $CuNMn_3$. *Solid State Commun.* **2001**, *120*, 307–310.
(100) Wu, M.; Wang, C.; Sun, Y.; Chu, L.; Yan, J.; Chen, D.; Huang, Q.; Lynn, J. W. Magnetic Structure and Lattice Contraction in Mn_3NiN. *J. Appl. Phys.* **2013**, *114*, 123902–123907.
(101) Fruchart, D.; Givord, D.; Convert, P.; Heritier, P.; Senateur, J. P. The Non-Collinear Component in the Magnetic Structure of Mn_4N. *J. Phys. F Met. Phys.* **1979**, *9*, 2431–2437.
(102) Uehara, M.; Yamazaki, T.; Kori, T.; Kashida, T.; Kimishima, Y.; Hase, I. Superconducting Properties of $CdCNi_3$. *J. Phys. Soc. Japan* **2007**, *76*, 034714–034718.
(103) He, B.; Dong, C.; Yang, L.; Chen, X.; Ge, L. $CuNNi_3$: A New Nitride Superconductor with Antiperovskite Structure. *Supercond. Sci. Technol.* **2013**, *26*, 125015–125020.
(104) Uehara, M.; Uehara, A.; Kozawa, K.; Yamazaki, T.; Kimishima, Y. New Antiperovskite Superconductor $ZnNNi_3$, and Related Compounds. *Physica C* **2010**, *470*, S688–S690.
(105) Nagakaru, S.; Otsuka, N.; Hirotsu, Y. Electron State of Ni_4N Studied by Electron Diffration. *J. Phys. Soc. Japan* **1973**, *35*, 1492–1495.
(106) Sun, Y.; Guo, Y.; Tsujimoto, Y.; Wang, X.; Li, J.; Sathish, C. I.; Wang, C.; Yamaura, K. Thermodynamic, Electromagnetic, and Lattice Properties of Antiperovskite Mn_3SbN. *Adv. Condens. Matter Phys.* **2013**, *10*, 1–5.
(107) Takata, F.; Ito, K.; Higashikozono, S.; Gushi, T.; Toko, K.; Suemasu, T. Epitaxial Growth and Magnetic Properties of $Ni_xFe_{4-x}N$ (X = 0, 1, 3, and 4) Films on $SrTiO_3$(001) Substrates. *J. Appl. Phys.* **2016**, *120*, 083907–083913.
(108) Holleck, H. Carbon- and Boron-Stabilized Ordered Ihases of Scandium. *J. Less-Common Met.* **1977**, *52*, 167–172.
(109) Kenmotsu, A.; Shinohara, T.; Watanabe, H. Nuclear Magnetic Resonance of Ferromagnetic Mn_3AlC and Mn_3GaC. *J. Phys. Soc. Japan* **1972**, *32*, 377–381.
(110) Deng, S.; Sun, Y.; Wang, L.; Shi, Z.; Wu, H.; Huang, Q.; Yan, J.; Shi, K.; Hu, P.; Zaoui, A.; et al. Frustrated Triangular Magnetic Structures of Mn_3ZnN: Applications in Thermal Expansion. *J. Phys. Chem. C* **2015**, *119*, 24983–24990.